

Observation of the Vacuum-Rabi Spectrum for One Trapped Atom

A. Boca, R. Miller, K. M. Birnbaum, A. D. Boozer, J. McKeever, and H. J. Kimble

*Norman Bridge Laboratory of Physics 12-33
California Institute of Technology, Pasadena, CA 91125*

(Dated: October 23, 2018)

The transmission spectrum for one atom strongly coupled to the field of a high finesse optical resonator is observed to exhibit a clearly resolved vacuum-Rabi splitting characteristic of the normal modes in the eigenvalue spectrum of the atom-cavity system. A new Raman scheme for cooling atomic motion along the cavity axis enables a complete spectrum to be recorded for an individual atom trapped within the cavity mode, in contrast to all previous measurements in cavity QED that have required averaging over many atoms.

A cornerstone of optical physics is the interaction of a single two-level atom with the electromagnetic field of a high quality resonator. Of particular importance is the regime of strong coupling, for which the frequency scale g associated with reversible evolution for the atom-cavity system exceeds the rates (γ, κ) for irreversible decay of atom and cavity field, respectively [1]. In the domain of strong coupling, a photon emitted by the atom into the cavity mode is likely to be repeatedly absorbed and re-emitted at the single-quantum Rabi frequency $2g$ before being irreversibly lost into the environment. This oscillatory exchange of excitation between atom and cavity field results from a normal mode splitting in the eigenvalue spectrum of the atom-cavity system [2] which is manifest in emission [3] and absorption [4] spectra, and has been dubbed the vacuum-Rabi splitting [3].

Strong coupling in cavity QED as evidenced by the vacuum-Rabi splitting provides enabling capabilities for quantum information science, including for the implementation of scalable quantum computation [5, 6], for the realization of distributed quantum networks [7, 8], and more generally, for the study of open quantum systems [9]. Against this backdrop, experiments in cavity QED have made great strides over the past two decades to achieve strong coupling [10]. The vacuum-Rabi splitting for single intracavity atoms has been observed with atomic beams in both the optical [11, 12, 13] and microwave regimes [14]. The combination of laser cooled atoms and large coherent coupling has enabled single atomic trajectories to be monitored in real time with high signal-to-noise ratio, so that the vacuum-Rabi spectrum could be obtained from atomic transit signals produced by single atoms [15]. A significant advance has been the trapping of individual atoms in an optical cavity in a regime of strong coupling [16, 17], with the vacuum-Rabi splitting first evidenced for single trapped atoms in Ref. [16] and the entire transmission spectra recorded in Ref. [18].

Without exception these prior single atom experiments related to the vacuum-Rabi splitting in cavity QED [11, 12, 13, 14, 15, 16, 17, 18] have required averaging over trials with many atoms to obtain quantitative spec-

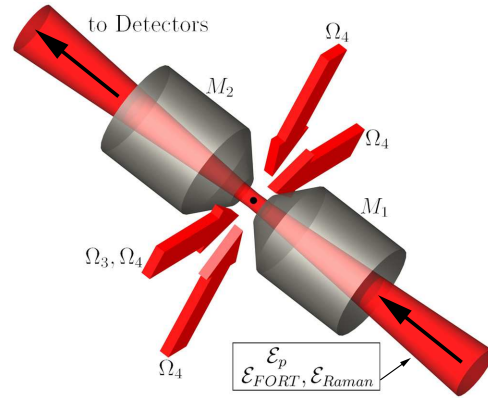


FIG. 1: A single atom is trapped inside an optical cavity in the regime of strong coupling by way of an intracavity FORT driven by the field \mathcal{E}_{FORT} . The transmission spectrum $T_1(\omega_p)$ for the atom-cavity system is obtained by varying the frequency ω_p of the probe beam \mathcal{E}_p and recording the output with single-photon detectors. Cooling of the radial atomic motion is accomplished with the transverse fields Ω_4 , while axial cooling results from Raman transitions driven by the fields \mathcal{E}_{FORT} , \mathcal{E}_{Raman} . An additional transverse field Ω_3 acts as a repumper during probe intervals.

tral information, even if individual trials involved only single atoms (e.g., 10^5 atoms were required to obtain a spectrum in Ref. [14] and $> 10^3$ atoms were needed in Ref. [18]). By contrast, the implementation of complex algorithms in quantum information science requires the capability for repeated manipulation and measurement of an individual quantum system, as has been spectacularly demonstrated with trapped ions [19, 20] and recently with Cooper pair boxes [21].

With this goal in mind, in this Letter we report measurements of the spectral response of single atoms that are trapped and strongly coupled to the field of a high finesse optical resonator. By alternating intervals of probe measurement and of atomic cooling, we record a complete probe spectrum for one and the same atom. The vacuum-Rabi splitting is thereby measured in a quantitative fashion for each atom by way of a protocol that represents a

first step towards more complex tasks in quantum information science. An essential component of our protocol is a new Raman scheme for cooling atomic motion along the cavity axis, that leads to inferred atomic localization $\Delta z_{axial} \simeq 33$ nm, $\Delta \rho_{transverse} \simeq 5.5$ μ m.

A simple schematic of our experiment is given in Fig. 1, with technical details provided in Ref. [22]. After release from a magneto-optical trap (MOT) located several mm above the Fabry-Perot cavity formed by mirrors (M_1, M_2), single Cesium atoms are cooled and loaded into an intracavity far-off-resonance trap (FORT) and are thereby strongly coupled to a single mode of the cavity. Our experiment employs the $6S_{1/2}, F = 4 \rightarrow 6P_{3/2}, F' = 5'$ transition of the $D2$ line in Cs at $\lambda_A = 852.4$ nm, for which the maximum single-photon Rabi frequency $2g_0/2\pi = 68$ MHz for ($F = 4, m_F = \pm 4$) \rightarrow ($F' = 5', m'_F = \pm 5$). The transverse decay rate for the $6P_{3/2}$ atomic excited states is $\gamma/2\pi = 2.6$ MHz, while the cavity field decays at rate $\kappa/2\pi = 4.1$ MHz [23]. Our system is in the strong coupling regime of cavity QED $g_0 \gg (\gamma, \kappa)$ [1], with critical photon and atom numbers $n_0 \equiv \gamma^2/(2g_0^2) \approx 0.0029$ and $N_0 \equiv 2\kappa\gamma/g_0^2 \approx 0.018$.

The intracavity FORT is driven by a linearly polarized input field \mathcal{E}_{FORT} at $\lambda_F = 935.6$ nm [24], resulting in nearly equal ac-Stark shifts for all Zeeman states in the $6S_{1/2}, F = 3, 4$ manifold [25]. At an antinode of the field, the peak value of the trapping potential for these states is $U_0/h = -39$ MHz for all our measurements. Zeeman states of the $6P_{3/2}, F' = 5'$ manifold likewise experience a trapping potential, albeit with a weak dependence on m'_F [17]. The cavity length is independently stabilized to length $l_0 = 42.2$ μ m such that a TEM_{00} mode at λ_{C_1} is resonant with the free-space atomic transition at λ_A and another TEM_{00} mode at λ_{C_2} is resonant at λ_F . The cavity waists are $w_{C_{1,2}} = \{23.4$ μ m, 24.5 μ m $\}$ at $\lambda_{C_{1,2}} = \{852.4$ nm, 935.6 nm $\}$.

As illustrated in Fig. 1, we record the transmission spectrum $T_1(\omega_p)$ for a weak external probe \mathcal{E}_p of variable frequency ω_p incident upon the cavity containing one strongly coupled atom [26]. Our protocol consists of an alternating sequence of probe and cooling intervals. The probe beam is linearly polarized [27] and is matched to the TEM_{00} mode around λ_{C_1} . \mathcal{E}_p illuminates the cavity for $\Delta t_{probe} = 100$ μ s, and the transmitted light is detected by two avalanche photodiodes for photon counting [28]. During this interval a repumping beam Ω_3 , transverse to the cavity axis, of frequency resonant with $6S_{1/2}, F = 3 \rightarrow 6P_{3/2}, F' = 4'$, also illuminates the atom. In successive probe intervals, the frequency ω_p of the probe beam is swept with an approximately linear ramp from well below to far above the common atom-cavity resonance at $\omega_A \simeq \omega_{C_1}$. The frequency sweep for the probe beam is repeated eight times in $\Delta t_{tot} = 1.2$ s, and then a new loading cycle is initiated.

Following each probe interval, we apply light to cool both the radial and axial motion for $\Delta t_{cool} = 2.9$ ms.

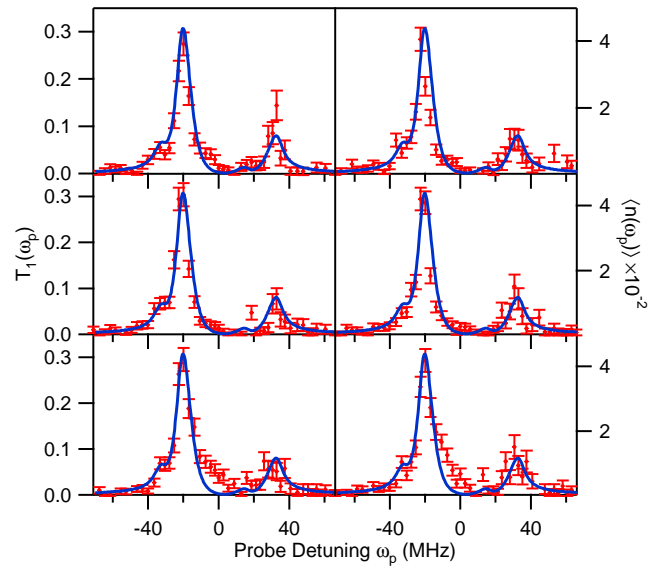


FIG. 2: Transmission spectrum $T_1(\omega_p)$ for six randomly drawn atoms [26]. In each case, $T_1(\omega_p)$ is acquired for one-and-the-same atom, with the two peaks of the vacuum-Rabi spectrum clearly evident. The error bars reflect the statistical uncertainties in the number of photocounts. The full curve is from the steady-state solution to the master equation as discussed in the text.

Radial cooling is achieved by the Ω_4 beams consisting of two pairs of counter-propagating fields in a σ_{\pm} configuration perpendicular to the cavity axis, as shown in Fig. 1. The Ω_4 beams are detuned $\Delta_4 \simeq 10$ MHz to the *blue* of the $4 \rightarrow 4'$ transition to provide blue Sisyphus cooling [29] for atomic motion transverse to the cavity axis.

To cool the axial motion for single trapped atoms, we have developed a new scheme that employs \mathcal{E}_{FORT} and an auxiliary field \mathcal{E}_{Raman} that is frequency offset by $\Delta_{Raman} = \Delta_{HF} + \delta$ and phase locked to \mathcal{E}_{FORT} . Here, $\Delta_{HF} = 9.192632$ GHz is the hyperfine splitting between the $6S_{1/2}, F = 3, 4$ levels and δ is a detuning. \mathcal{E}_{FORT} , \mathcal{E}_{Raman} generate intracavity fields with Rabi frequencies Ω_{FORT} , Ω_{Raman} that drive Raman transitions between the $F = 3, 4$ levels with effective Rabi frequency $\Omega_E \approx \Omega_{FORT}\Omega_{Raman}/(2\Delta)$, where in a simple theory the detuning $\Delta = \omega_A - \omega_{FORT}$. In our experiments, $\Omega_E \sim 200$ kHz. By tuning δ near the $\Delta n = -2$ motional sideband (i.e., $-2\nu_0 \sim \delta = -1.0$ MHz with ν_0 as the vibrational frequency for harmonic motion in the axial direction around an antinode of the FORT), we implement sideband cooling via the $F = 3 \rightarrow 4$ transition, with repumping provided by the radial Ω_4 beams. Note that the Raman process also acts as a repumper for population pumped to the $F = 3$ level by the Ω_4 beams. Each cooling interval is initiated by turning on the fields Ω_4 , \mathcal{E}_{Raman} during Δt_{cool} and is terminated by gating these fields off before the next probe interval Δt_{probe} .

Figure 2 displays the normalized transmission spectra

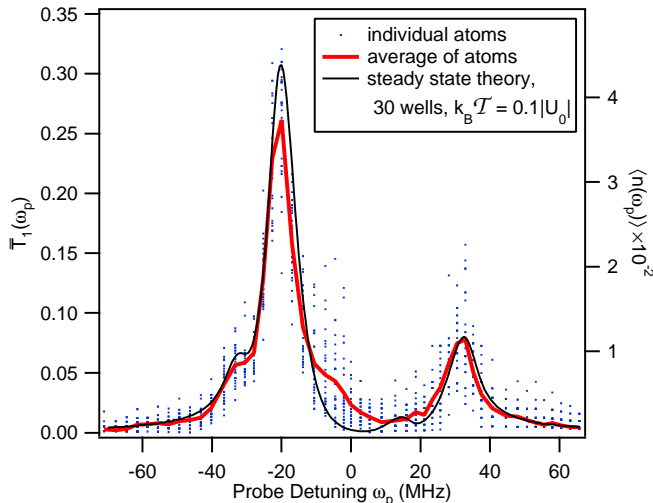


FIG. 3: Transmission spectrum $\bar{T}_1(\omega_p)$ resulting from averaging individual spectra for $N = 28$ atoms as in Fig. 1 [26]. The points are a scatter plot from the data for $T_1(\omega_p)$ for all 28 atoms. The thin trace is from the steady-state solution to the master equation, and is identical to that in Fig. 2. The only free parameters in the theory are the temperature and the range of FORT antinodes; the vertical scale is absolute.

T_1 [26] for individual atoms acquired by way of our protocol of alternating probe and cooling intervals. Clearly evident in each trace is a two-peaked structure that represents the vacuum-Rabi splitting observed on an atom-by-atom basis. For comparison, also shown in the figure is the predicted transmission spectrum obtained from the steady-state solution to the master equation for one atom strongly coupled to the cavity, as discussed below. The quantitative correspondence between theory and experiment is evidently quite reasonable for each atom [30].

To obtain the data shown in Fig. 2, $N_{load} = 61$ atoms were loaded into the FORT in 500 attempts, with the probability that a given successful attempt involved 2 or more atoms estimated to be $P_{load}(N \geq 2) \lesssim 0.06$. Of these 61 atoms, $N_{survive} = 28$ atoms remained trapped for the entire duration Δt_{tot} of the measurement of $T_1(\omega_p)$. The six spectra shown in Fig. 2 were selected by a random drawing from this set of $N_{survive}$ atoms. Our sole selection criterion for presence of an atom makes no consideration of the spectral structure of $T_1(\omega_p)$ except that there should be large absorption on line center, $T_1(\omega_p = \omega_{C_1}) \leq T_{thresh} \approx 0.2$, with $T_0(\omega_p = \omega_{C_1}) \equiv 1$ for the empty cavity [31]. Note that the lifetime for an atom trapped in the FORT in the absence of the cooling and probing light is $\tau_0 \simeq 3$ s, which leads to a survival probability $p(\Delta t_{tot}) \simeq 0.7$.

In Fig. 3 we collect the results for $T_1(\omega_p)$ for all $N_{survive} = 28$ atoms, and display the average transmission spectrum $\bar{T}_1(\omega_p)$, as well a scatter plot from the individual spectra. This comparison demonstrates that the vacuum-Rabi spectrum observed for any particular

atom represents with reasonable fidelity the spectrum that would be obtained from averaging over many atoms, albeit with fluctuations due to Poisson counting and optical pumping effects over the finite duration of the probe. Note that the total acquisition time associated with the probe beam for the spectrum of any one atom is only 40 ms, which can be improved as we optimize the cooling protocol to give better statistics for each atom.

We have also acquired transmission spectra $T_1(\omega_p)$ under operating conditions beyond those displayed in Figs. 2, 3, including drive intensities $|\mathcal{E}_p|^2$ varied by factors of 2, $\frac{1}{2}$, and $\frac{1}{4}$, and atom-cavity detunings $\Delta_{AC} = \omega_A - \omega_{C_1} = \pm 13$ MHz. In all cases, we observe a distinctive vacuum-Rabi splitting on an atom-by-atom basis, and will discuss the quantitative comparison of these results with theory elsewhere [32].

The full curves in Figs. 2, 3 are obtained from the steady state solution of the master equation including all transitions $(F = 4, m_F) \leftrightarrow (F' = 5', m'_F)$ with their respective coupling coefficients $g_0^{(m_F, m'_F)}$, as well as the two nearly degenerate modes of our cavity [24, 27]. For the comparison of theory and experiment, the parameters $(g_0^{(m_F, m'_F)}, \gamma, \kappa, \omega_{C_1}, \omega_p, |\mathcal{E}_p|^2, U_0)$ are known in absolute terms without adjustment. However, we have no *a priori* knowledge of the particular FORT well into which the atom is loaded along the cavity standing wave, nor of the energy of the atom. The FORT shifts and coherent coupling rate are both functions of atomic position \mathbf{r} , with $U(\mathbf{r}) = U_0 \sin^2(k_{C_2} z) \exp(-2\rho^2/w_{C_2}^2)$ and $g^{(m_F, m'_F)}(\mathbf{r}) = g_0^{(m_F, m'_F)} \psi(\mathbf{r})$, where $g_0^{(m_F, m'_F)} = g_0 G_{m_F, m'_F}$ with $G_{i,f}$ related to the Clebsch-Gordan coefficient for the particular $m_F \leftrightarrow m'_F$ transition. $\psi(\mathbf{r}) = \sin(k_{C_1} z) \exp(-\rho^2/w_{C_1}^2)$, where ρ is the transverse distance from the cavity axis z , and $k_{C_{1,2}} = 2\pi/\lambda_{C_{1,2}}$.

As discussed in connection with Fig. 4 below, for the theoretical curves shown in Figs. 2, 3, we have chosen only the 30 out of 90 total FORT wells for which $|\psi(\mathbf{r}_{FORT})| \geq 0.87$, where \mathbf{r}_{FORT} specifies a maximum for the FORT intensity (i.e., $U(\mathbf{r}_{FORT}) = U_0$). Furthermore, for these wells we have averaged $T_1(\omega_p)$ over a Gaussian distribution in position \mathbf{r} consistent with a temperature $k_B \mathcal{T} = 0.1 U_0$ (~ 200 μ K). Since all parameters are known except for those that characterize atomic motion, the good agreement between theory and experiment [33] allows us to infer that our cooling protocol together with the selection criterion $T_{thresh} = 0.2$ results in individual atoms that are strongly coupled in one of the “best” FORT wells (i.e., $|\psi(\mathbf{r}_{FORT})| \gtrsim 0.87$) with “temperature” ~ 200 μ K [34].

In support of these assertions, Fig. 4(a) explores the theoretical dependence of the transmission spectrum $T_1(\omega_p)$ on the set of FORT wells selected, and hence on the distribution of values for $|\psi(\mathbf{r}_{FORT})|$ in the ideal case $\mathcal{T} = 0$. Extending the average beyond the 30 “best” FORT wells (i.e., $|g(\mathbf{r}_{FORT})|/g_0 \lesssim 0.87$) leads

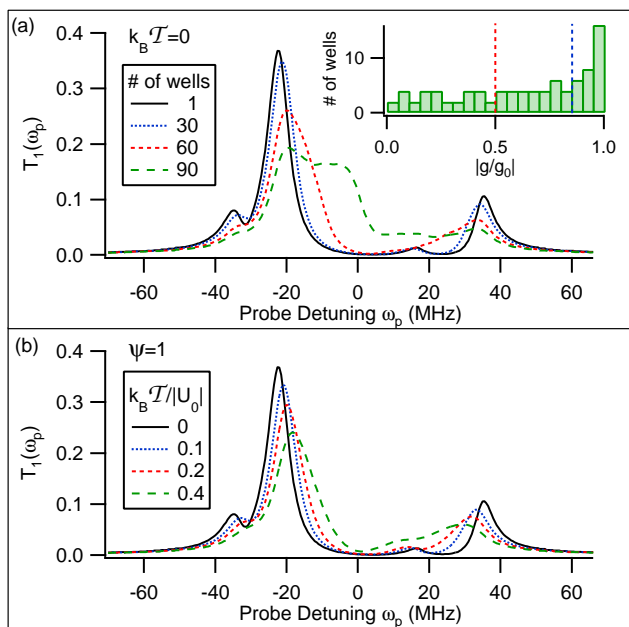


FIG. 4: Theoretical plots for $T_1(\omega_p)$ from the steady-state solution to the master equation. (a) For zero temperature, $T_1(\omega_p)$ is calculated from an average over various FORT antinodes along the cavity axis, with the inset showing the associated distribution of values for $|g(\mathbf{r}_{\text{FORT}})|/g_0$. (b) For an optimum FORT well (i.e., $|g(\mathbf{r}_{\text{FORT}})|/g_0 = 1$), $T_1(\omega_p)$ is computed for various temperatures from an average over atomic positions within the well.

to spectra that are inconsistent with our observations in Figs. 2, 3. Figure 4(b) likewise investigates the dependence of $\bar{T}_1(\omega_p)$ on the temperature \mathcal{T} for an atom trapped in the “best” well (i.e., $|\psi(\mathbf{r}_{\text{FORT}})| = 1$). For temperatures $\mathcal{T} \gtrsim 200 \mu\text{K}$, the calculated spectra are at variance with the data in Figs. 2, 3, from which we infer atomic localization $\Delta z \simeq 33 \text{ nm}$ in the axial direction and $\Delta x = \Delta y \simeq 3.9 \mu\text{m}$ in the plane transverse to the cavity axis. Beyond these conclusions drawn from Figs. 2–4, a consistent feature of all our measurements is that reasonable correspondence between theory and experiment is only obtained by restricting $|\psi(\mathbf{r})| \gtrsim 0.8$.

Our experiment represents an important advance in the quest to obtain single atoms trapped with optimal strong coupling to a single mode of the electromagnetic field. The vacuum-Rabi splitting is the hallmark of strong coupling for single atoms and photons, and all measurements until now have required averaging over many atoms for its observation. By contrast, we are able to observe spectra $T_1(\omega_p)$ on an atom-by-atom basis with clearly resolved normal-mode splittings. These spectra contain detailed quantitative information about the coherent coupling $g(\mathbf{r})$ and FORT shifts for each atom. This information indicates that the coupling g is in a narrow range of near-maximal values. Our observations are made possible by the implementation of a new scheme

to cool both the radial and axial atomic motion. The capabilities demonstrated in this Letter should provide the tools necessary to implement diverse protocols in quantum information science [5, 6, 7, 8, 9].

We gratefully acknowledge the contributions of T. Northup. This research is supported by the Caltech MURI Center for Quantum Networks, by the National Science Foundation, and by the Advanced Research and Development Activity (ARDA).

-
- [1] H. J. Kimble, *Physica Scripta* **T76**, 127 (1998).
 - [2] E. T. Jaynes and F. W. Cummings, *Proc. IEEE* **51**, 89 (1963).
 - [3] J. J. Sanchez-Mondragon, N. B. Narozhny, and J. H. Eberly, *Phys. Rev. Lett.* **51**, 550 (1983).
 - [4] G. S. Agarwal, *Phys. Rev. Lett.* **53**, 1732 (1984).
 - [5] T. Pellizzari, S. A. Gardiner, J. I. Cirac, and P. Zoller, *Phys. Rev. Lett.* **75**, 3788 (1995).
 - [6] L.-M. Duan and H. J. Kimble, *Phys. Rev. Lett.* **92**, 127902 (2004)
 - [7] J. I. Cirac, P. Zoller, H. J. Kimble, and H. Mabuchi, *Phys. Rev. Lett.* **78**, 3221 (1997).
 - [8] H.-J. Briegel *et al.*, in *The Physics of Quantum Information*, edited by D. Bouwmeester, A. Ekert and A. Zeilinger, p. 192.
 - [9] H. Mabuchi and A. C. Doherty, *Science* **298**, 1372 (2002).
 - [10] *Cavity Quantum Electrodynamics*, ed. P. Berman (Academic Press, San Diego, 1994).
 - [11] R. J. Thompson, G. Rempe, and H. J. Kimble, *Phys. Rev. Lett.* **68**, 1132 (1992).
 - [12] J. J. Childs *et al.*, *Phys. Rev. Lett.* **77**, 2901 (1996).
 - [13] R. J. Thompson, Q. A. Turchette, O. Carnal, and H. J. Kimble, *Phys. Rev. A* **57**, 3084 (1998).
 - [14] M. Brune *et al.*, *Phys. Rev. Lett.* **76**, 1800 (1996).
 - [15] C. J. Hood, M. S. Chapman, T. W. Lynn, and H. J. Kimble, *Phys. Rev. Lett.* **80**, 4157 (1998).
 - [16] J. Ye, D. W. Vernooy, and H. J. Kimble, *Phys. Rev. Lett.* **83**, 4987 (1999).
 - [17] J. McKeever *et al.*, *Phys. Rev. Lett.* **90**, 133602 (2003).
 - [18] P. Maunz *et al.*, *quant-ph/0406136*.
 - [19] M. Riebe *et al.*, *Nature* **429**, 734 (2004).
 - [20] M. D. Barrett *et al.*, *Nature* **429**, 737 (2004).
 - [21] A. Wallraff *et al.*, *Nature* **431**, 162 (2004); I. Chiorescu *et al.*, *ibid.*, 159.
 - [22] J. McKeever, Doctoral Dissertation (California Institute of Technology, 2004).
 - [23] C. J. Hood, J. Ye, and H. J. Kimble, *Phys. Rev. A* **64**, 033804 (2001).
 - [24] Stress-induced birefringence in the cavity mirrors [23] leads to two nondegenerate cavity modes with orthogonal polarizations \hat{l}_{\pm} and with mode splitting $\Delta\nu_{C_1} = 4.4 \pm 0.2 \text{ MHz}$. $\mathcal{E}_{\text{FORT}}$, $\mathcal{E}_{\text{Raman}}$ are linearly polarized and aligned along \hat{l}_{+} for the higher frequency mode.
 - [25] K. L. Corwin *et al.*, *Phys. Rev. Lett.* **83**, 1311 (1999).
 - [26] $T_1(\omega_p)$ is proportional to the ratio of photon flux transmitted by M_2 to the flux $|\mathcal{E}_p|^2$ incident upon M_1 and is normalized such that the transmission $T_0(\omega_{C_1}) \equiv 1$ for the empty cavity at line center. Figs. 2, 3 also show $\langle n(\omega_p) \rangle$, the corresponding intracavity photon number.

- [27] Relative to the polarization eigen-axes \hat{l}_\pm of the two cavity modes, the linear polarization vector \hat{l}_p for the probe field \mathcal{E}_p is aligned along a direction $\hat{l}_p = \cos\theta\hat{l}_+ + \sin\theta\hat{l}_-$, where $\theta = 13^\circ$ for Fig. 2; however, both theory and experiment are relatively insensitive to θ for $\theta \lesssim 15^\circ$.
- [28] The efficiency for photon escape from the cavity is $\alpha_{e2} = 0.6 \pm 0.1$. The propagation efficiency from M_2 to detectors (D_1, D_2) is $\alpha_P = 0.41 \pm .03$, with then each detector receiving half of the photons. (D_1, D_2) have quantum efficiencies $\alpha_P = 0.49 \pm 0.05$.
- [29] D. Boiron *et al.*, Phys. Rev. A **53**, R3734 (1996) and references therein.
- [30] The maximum ac-Stark shifts of the ($F' = 5', m'_F$) states are given by $\{m'_F, U_{m'_F}\} = \{\pm 5, 1.18U_0\}, \{\pm 4, 1.06U_0\}, \{\pm 3, 0.97U_0\}, \{\pm 2, 0.90U_0\}, \{\pm 1, 0.86U_0\}, \{0, 0.85U_0\}$. These Stark shifts in conjunction with optical pumping caused by \mathcal{E}_p lead to the asymmetric peak heights observed in Figs. 2, 3 via an effective population-dependent shift of the atomic resonance frequency.
- [31] Transmission spectra $T_1(\omega_p), \bar{T}_1(\omega_p)$ are insensitive over a range of selection criteria $0.02 \leq T_{thresh} \leq 0.73$.
- [32] K. M. Birnbaum *et al.*, in preparation.
- [33] In Figs. 2, 3, the discrepancy between experiment and the *steady-state* theory for $\bar{T}_1(\omega_p)$ around $\omega_p \sim 0$ can be accounted for by a *transient* solution to the master equation which includes optical pumping effects over the probe interval Δt_{probe} .
- [34] Although the spectra are consistent with a thermal distribution, we do not exclude a more complex model involving probe-dependent heating and cooling effects.